

Joint Ultra-wideband and Signal Strength-based Through-building Tracking for Tactical Operations

Merrick McCracken, Maurizio Bocca, and Neal Patwari

Electrical and Computer Engineering Department

University of Utah, Salt Lake City, Utah, USA

Email: merrick.mccracken@gmail.com, maurizio.bocca@utah.edu, npatwari@ece.utah.edu

Abstract—Accurate device free localization (DFL) based on received signal strength (RSS) measurements requires placement of radio transceivers on all sides of the target area. Accuracy degrades dramatically if sensors do not surround the area. However, law enforcement officers sometimes face situations where it is not possible or practical to place sensors on all sides of the target room or building. For example, for an armed subject barricaded in a motel room, police may be able to place sensors in adjacent rooms, but not in front of the room, where the subject would see them. In this paper, we show that using two ultra-wideband (UWB) impulse radios, in addition to multiple RSS sensors, improves the localization accuracy, particularly on the axis where no sensors are placed (which we call the x -axis). We introduce three methods for combining the RSS and UWB data. By using UWB radios together with RSS sensors, it is still possible to localize a person through walls even when the devices are placed only on two sides of the target area. Including the data from the UWB radios can reduce the localization area of uncertainty by more than 60%.

Index Terms—Device-free localization, ultra-wideband, radio tomographic imaging, hidden Markov model, bistatic radar

I. INTRODUCTION

Device free localization (DFL) systems can be used in tactical operations or crisis situations to help emergency personnel know where people are in a room or building before they enter [1]. These systems do not require people to participate in the localization effort by wearing or carrying sensors or radio devices. Radio frequency (RF) measurements are appropriate for emergency operations because RF penetrates (non-metal) walls. Such through-wall sensing could benefit police during hostage or barricade situations. However, in many such situations, it is not possible to place sensors on all sides of the building or area. For example, some sides of a building might have windows where an armed subject may be watching, and deploying sensors on that side could expose police to harm or escalating the situation. As another example, a room on an upper floor of a building may have some accessible interior walls (e.g., in a hallway), but the exterior wall may be inaccessible simply because of its height. This paper provides a system that expands the possibilities for RF-based DFL systems where an area cannot be surrounded with sensors by combining RSS-based DFL methods with bistatic ultra-wideband (UWB) impulse radar methods.

We are particularly motivated by discussions with our local SWAT team, who have unfortunately, faced three situations in as many years in our metro area [2], [3], [4] in which hostages

were taken by a barricaded subject in a hotel or motel room. Knowing the location of the suspect represents very valuable information in planning the actions (e.g., forced entry) required to bring the standoff to an end safely. In such situations, sensors could be placed in adjacent rooms to the barricaded room, but rooms have front windows, and sometimes back windows, thus front and back walls are potentially off-limits.

A DFL system based on received signal strength (RSS) measurements [5], [6], [7], [8] typically has radio transceivers, which we call *RSS sensors* placed on all four sides of a target area. Measured RSS between every pair of sensors are used to estimate the location of the person in the room in real-time. The localization process is based on models for the change in RSS introduced by the presence of a person on or near the *link line*, i.e., the straight imaginary line connecting the transmitter and receiver [6], [9], [10]. When RSS sensors are placed only on two opposite sides of a room, the links cross the monitored area along one axis but not the other. This significantly degrades the localization accuracy of the system, especially along the axis with no crossing links [6].

UWB radios can be used for DFL through walls and can be accurate on the order of centimeters or tens of cm [11], [12]. Multiple UWB radios cooperating in a multistatic radar configuration can provide an unambiguous localization estimate [11]. A transmitter broadcasts a UWB impulse and receivers capture the time-domain channel impulse response (CIR) of the environment. Changes to the CIR are detected and the time delay beyond the line-of-sight (LoS) pulse for each of these changes is used to estimate the range of the target from the radios [13]. These radios, however, can be prohibitively expensive to install on a permanent basis: a single UWB impulse radio can cost thousands of dollars, and using only a single pair of radios provides insufficient information to unambiguously localize a target.

In this paper, we introduce a joint DFL system that uses the changes measured in RSS and CIR to localize and track a target, such as a person, through walls. We demonstrate, in particular, the localization accuracy of a system which deploys sensors only on two opposite sides of a room. We call the axis parallel to the sides of the room without sensors the X axis and the axis parallel to the sides of the room with sensors the Y axis (see Figures 1 and 2). The RSS sensors primarily provide the information about the target's y coordinate, while the UWB radios primarily provide information about the target's

x coordinate. This removes the need to have RSS sensors on all four sides of a target room and reduces the number of UWB radios required for localization. We introduce methods to process and combine the RSS and CIR data in order to provide a unique position estimate. We also propose methods that do not require an initial calibration of the system. The experimental results collected in two deployments, *i.e.*, a study room at the University of Utah and a motel room in Salt Lake City, show that the joint RSS-UWB DFL system can accurately localize a non-cooperative target through walls. Even when the number of deployed devices is low, *e.g.*, only two UWB radios and six (three per side) RSS sensors, the system can still provide a position estimate accurate enough to reliably indicate in which part of the room the person is located. In tactical situations where the only opportunity to have access to the target room is to open a breach in a wall with an explosive frame, this information can be used by police forces to decide which wall has to be detonated and avoid hurting or killing the suspect.

In tactical operations or crisis situations, law enforcement may not have the possibility of calibrating the systems used for DFL in stationary conditions, *i.e.*, when no person is located in the target area. The methods used to process the data coming from the RSS sensors and UWB radios should be able to localize and track the suspect in the room from the start, making DFL a *plug-and-play* type of system. In this paper, we propose novel variance-based methods for RSS and CIR measurements that can localize the person without requiring an initial calibration of the system in stationary conditions.

At the time of writing, there are several commercially available through-wall radio technologies that can help law enforcement determine the position of people inside a room. The Prism200 from Cambridge Consultants [14] is a through-wall radar system for determining the location and movement of people for law enforcement or emergency personnel. The XaverTM products from Camero are also through-wall UWB solutions that provide similar capabilities [15]. Time Domain is another company that offers solutions for target localization and tracking using UWB radios [16]. The UWB radios used in this work are a pair of P220 UWB radios from Time Domain. Compared to these products, the joint RSS-UWB DFL system described in this paper is considerably less expensive, as the RSS sensors cost few tens of dollars each and only two UWB radios are required. Moreover, the compact size and low weight of the RSS sensors and UWB radios make our system easier to be installed.

The paper is organized as follows. In Section II, we describe the radio tomographic imaging (RTI) technique used to process the RSS measurements coming from the RSS sensors. In Section III, we describe the methods used for estimating the bistatic range of a target using UWB radios by modeling the changes to the CIR as a hidden Markov model. Section IV introduces three methods to combine the RSS and CIR data in order to provide a unique position estimate. Section VI describes the experiments carried out, while Section VII presents the results and compare the performance of the

different methods. Conclusions are given in Section VIII.

II. RADIO TOMOGRAPHIC IMAGING (RTI)

In RTI, originally introduced in [6], radio transceivers placed at known positions form a wireless mesh network and collect RSS measurements that can be used to localize and track a person in real-time without requiring her to wear or carry any sensor or radio device. RTI can provide sub-meter localization accuracy, also in through-wall scenarios [1], [17], [18]. The RSS measurements of all the links of the network are processed in order to estimate a discretized image \mathbf{x} of the change in the propagation field of the monitored area caused by the presence a person. The estimation problem can be defined as:

$$\mathbf{y} = \mathbf{W}\mathbf{x} + \mathbf{n}, \quad (1)$$

in which \mathbf{y} and \mathbf{n} are $L \times 1$ vectors of the RSS measurements and noise of the L links of the network, respectively, and \mathbf{x} is the $N \times 1$ image to be estimated, where N is the number of voxels of the image. Each element x_n of \mathbf{x} represents the change in the propagation field due to the presence of a person in voxel n . The $L \times N$ weight matrix \mathbf{W} represents a spatial impact model between the L links of the network and the N voxels of the image. The model used in RTI [1], [6], [9], [17] is an ellipse having the foci located at the transmitter and receiver of the the link. The voxels located within the ellipse have their weight set to a constant which is inversely proportional to the root distance between the transmitter and receiver, while the voxels located outside of the ellipse have their weight set to zero.

A. Attenuation-based RTI

For attenuation-based RTI, we use the method introduced in [17]. In this section, we briefly present this method and the terminology that will be used also in the following sections.

The RSS of link l on channel c at time instant k , $r_{l,c}(k)$, can be modeled as:

$$r_{l,c}(k) = P_c - L_{l,c} - S_{l,c}(k) + F_{l,c}(k) - \eta_{l,c}(k), \quad c \in \mathcal{F} \quad (2)$$

where P_c is the transmit power of the sensors, $L_{l,c}$ the large scale path loss, $S_{l,c}$ the shadowing loss, $F_{l,c}$ the fading gain (or *fade level* [10]), $\eta_{l,c}$ the measurement noise, and $\mathcal{F} = \{1, \dots, H\}$ is the set of measured frequency channels. Both the large scale path loss $L_{l,c}$ and the shadowing loss $S_{l,c}$ change very slowly with the center frequency. In our experiments, we use IEEE 802.15.4-compliant transceivers [19] which may transmit in one of 16 channels across the 2.4 GHz ISM band. Because the band, 80 MHz, is small compared to 2.4 GHz, we can assume that both $L_{l,c}$ and $S_{l,c}$ are independent of the frequency channel c . Consequently, $F_{l,c}$ can be calculated as:

$$F_{l,c}(k) = r_{l,c}(k) - P_c + \eta_{l,c}(k). \quad (3)$$

Due to the measurement noise $\eta_{l,c}$, the fade level can not be measured directly. Thus, we estimate it by using the average

RSS, $\bar{r}_{l,c}$, measured during an initial calibration of the system performed when no person is in the monitored area:

$$\bar{F}_{l,c} = \bar{r}_{l,c} - \min_c \bar{r}_{l,c}. \quad (4)$$

In [10], the links are divided in *anti-fade* and *deep fade* links depending on the change in RSS measured when a person crosses the *link line*, *i.e.* the imaginary straight line connecting the transmitter and receiver. A link is in a deeper fade on channel c_1 than on channel c_2 if $\bar{r}_{l,c_1} < \bar{r}_{l,c_2}$. By definition, $\bar{F}_{l,c} \geq 0$ and $\bar{F}_{l,c} = 0$ for one channel c on each link. Anti-fade links are the most informative for localization, since their spatial impact area is limited around the link line, while deep fade links measure a consistent change in RSS even when the person is far from the link line. For this reason, for each link l we calculate the fade level in (4) of each channel $c \in \mathcal{F}$, and we rank the measured frequency channels from the most anti-fade to the most deep fade. If \mathcal{A}_i is the set of size m containing the indices of the m top channels in the fade-level ranking, the link RSS measurement y_l at time k is calculated as:

$$y_l(k) = \frac{1}{m} \sum_{c \in \mathcal{A}_i} \Delta r_{l,c}(k), \quad (5)$$

where $\Delta r_{l,c}(k) = r_{l,c}(k) - \bar{r}_{l,c}$, *i.e.*, $\Delta r_{l,c}(k)$ is the difference between the current RSS measurement and the average RSS measured during the initial calibration phase.

B. Variance-based RTI

We present a new multi-channel version of variance-based RTI extending and improving the results of [1]. In this new method, we also include the concept of fade level. We calculate the mean of the RSS over a longer time window in order to better estimate the fade level of each frequency channel, and we use this mean to calculate the RSS short-term variance.

The attenuation-based RTI method in [17] requires an initial calibration of the system in stationary conditions, *i.e.*, when the monitored area is empty. Moreover, if the environment changes, *e.g.*, when the suspect in the room moves furniture or other objects, the RTI system would need to be recalibrated or would otherwise lose accuracy. The works in [18], [?] address this issue and introduce methods capable of estimating the baseline RSS of the links on-line.

In tactical operations, such as when an armed person has barricaded himself in a house or motel room before the arrival of police forces on the scene, we cannot expect to require an empty area. Variance-based RTI can be applied in this scenario. The change in RSS due to the presence of a person on the link line can be quantified as the unbiased sample variance of the last N_s RSS measurements:

$$\hat{s}_{l,c}(k) = \frac{1}{N_s - 1} \sum_{p=0}^{N_s-1} (r_{l,c}(k-p) - \mu_{l,c}(k))^2, \quad (6)$$

where:

$$\mu_{l,c}(k) = \frac{1}{N_\mu} \sum_{p=0}^{N_\mu-1} r_{l,c}(k-p) \quad (7)$$

TABLE I
RTI IMAGE ESTIMATION PARAMETERS

Description	Parameter	Value
Voxel width [m]	p	0.15
Ellipse excess path length [m]	λ	0.02
Voxels' variance [dB]	σ_x^2	0.05
Noise standard deviation [dB]	σ_N	1
Voxels' correlation distance	δ_c	4
Number of selected channels	m	3
Short-term RSS variance window	N_s	5
Long-term RSS mean window	N_μ	50
Empty area intensity threshold	T_e	0.05
Number of updates for confirmation	h_{app}	8
Confirmation window	H	15
Gating area radius [m]	ω	1.2

is the mean of the last N_μ RSS measurements of link l on channel c , where $N_\mu > N_s$ so to estimate the mean RSS of each channel on a longer time window and filter the changes due to the person crossing the link line. Variance-based RTI does not require an initial calibration of the system and can adapt at run-time to eventual changes in the environment. For each link l , $\mu_{l,c}(k)$ in (7) provides an estimate of the fade level of channel c at time k . As for attenuation-based RTI in Section II-A, the channels are ranked from the most anti-fade to the most deep fade. The link measurement y_l at time k is calculated as:

$$y_l(k) = \frac{1}{m} \sum_{c \in \mathcal{A}_i} \hat{s}_{l,c}(k). \quad (8)$$

C. RTI image estimation

Since the number of links L is considerably smaller than the number of voxels N , the estimation of the image \mathbf{x} is an ill-posed inverse problem that can be solved through regularization. In this work, we use a regularized least-squares approach [9], [20], [17], [18]. The discretized image of the change in the propagation field of the monitored area is calculated as:

$$\hat{\mathbf{x}} = \mathbf{\Pi} \mathbf{y}, \quad (9)$$

where $\mathbf{y} = [y_1, \dots, y_L]^T$, and

$$\mathbf{\Pi} = (\mathbf{W}^T \mathbf{W} + \mathbf{C}_x^{-1} \sigma_N^2)^{-1} \mathbf{W}^T, \quad (10)$$

in which σ_N is the regularization parameter. The *a priori* covariance matrix \mathbf{C}_x is calculated by using an exponential spatial decay:

$$[\mathbf{C}_x]_{ji} = \sigma_x^2 e^{-\|\mathbf{v}_j - \mathbf{v}_i\|/\delta_c}, \quad (11)$$

where σ_x^2 is the variance of voxel measurements, and δ_c is the voxels' correlation distance. The linear transformation $\mathbf{\Pi}$ is computed only once before the system starts operating in real-time. The calculation of $\hat{\mathbf{x}}$ in (9) requires $L \times N$ operations and can be performed in real-time. Table I indicates the values of the parameters of the RTI image estimation process.

III. ULTRA-WIDE BAND RANGE ESTIMATION

Assuming an UWB transmitter sends a pulse $\delta(t)$, each channel impulse response (CIR) is measured as:

$$h(t) = \sum_i \alpha_i \delta(t - \tau_i), \quad (12)$$

where α_i and τ_i are the complex amplitude and time delay of the i th multipath component, respectively. The line of sight path delay is τ_0 . The path delay of the target, which we wish to estimate, is τ_* . We will consider a discrete-sampled version of the signal energy, r_k :

$$r_k = \int_{(k-1/2)T}^{(k+1/2)T} |h(t)|^2 dt, \quad (13)$$

where T is the sampling period and k ranges from $1 \dots M$. In this work, $T = 1$ ns. From now on, CIR time delays will be considered only over discrete time intervals k rather than continuously on t .

A. Changes to the CIR as a Hidden Markov Model

The changes to the UWB CIR are modeled as a hidden Markov chain. We will refer to this method as *HMM-UWB* or hidden Markov model (HMM) based UWB. A hidden Markov chain is one whose states, $X_k = i$, are not directly observable but are inferred from other observation signals, O_k , available from the system. The distribution of the observation signals is dependent on the state of the system, *i.e.*, $f_{O,i} = P(O|X = i)$. To estimate the probability the system is in a given state at any time k , *i.e.*, $P(X_k = i|\mathbf{O}, \lambda)$, we need to know the distributions of the observation signals, the initial state probabilities π_i , and the state transition probabilities, $P_{i,j}$, all of which are described by $\lambda = [\pi_i, P_{i,j}, f_{O,i}]$ [21].

The observations, O_k , are the difference between the CIRs of the static environment and the CIRs of when a person is located in the monitored area. This difference is calculated as the symmetric Kullback-Leibler divergence, also known as relative entropy [22]. Assuming a Gaussian distribution for r_k over many CIRs, the closed form solution for the observed signal, O_k , is:

$$O_k = \frac{1}{2} \left(\frac{\sigma_p^2}{\sigma_q^2} + \frac{\sigma_q^2}{\sigma_p^2} + \frac{(\mu_p - \mu_q)^2 (\sigma_p^2 + \sigma_q^2)}{\sigma_p^2 \sigma_q^2} \right) - 1 \quad (14)$$

where μ_p and σ_p^2 are the mean and variance of r_k during the calibration period, and μ_q and σ_q^2 are the mean and variance of r_k when a person is located in the target area, respectively. The distribution of the observations is approximately a log-normal distribution [?].

If the changes to the CIR are modeled as a hidden Markov chain, the CIR goes from an unchanged state, $X = 0$, to a changed state, $X = 1$, at the time delay corresponding to the time traveled by the UWB pulse from the transmitter to reflect off of the target and then arrive at the receiving radio, *i.e.* k_* , which is equivalent to τ_* . By applying this model to the system, standard HMM solving algorithms, such as the forward-backward algorithm [21], can be used to estimate

when the system state changes and, thus, when changes to the CIR occur. The forward-backward algorithm determines the most likely state of the system at any given time as:

$$\hat{X}_k = \arg \max_i P(X_k = i|\mathbf{O}, \lambda). \quad (15)$$

These state estimates are used to estimate k_* as

$$P(X_k = 1|\mathbf{O}, \lambda) \leq 0.5 \} \hat{k}_* = \{k_* | \hat{X}_k \neq 1 \forall k < k_*\} \quad (16)$$

The work in [23] describes in further detail the method for estimating UWB bistatic range and its improved performance over other methods. From now on, we will let $\alpha_k = P(X_k = 1|\mathbf{O}, \lambda)$. α_k describes the probability those CIRs possibly affected by a person at time k are in the affected state. These probabilities are used to form the UWB localization image.

When solving the forward-backward algorithm, accurate estimates of when state changes occur is dependent on how well λ models the true system parameters. Often λ , and particularly the distribution of observation signals, is unknown when beginning to solve the forward-backward algorithm. A known λ from another environment can be used as an initial estimate for λ when solving for the state estimates. With more observations and state estimates as time progresses, the Baum-Welch algorithm can help tune λ to more closely match the true parameters and improve range estimates [21], [23].

It is critical that the observation vectors are accurate representations of the difference between a CIR with a possible target and the CIR of the known environment. This is a function of how well the calibration CIRs represent the static environment. Even as a person is walking in a room, something in the environment may change that can significantly affect the accuracy of the range estimates due to a change in the static environment. This includes changing the position of furniture or a door opening or closing. If the bistatic range of the change to the environment is closer than the target, it will not be possible to estimate the range of the target using the existing calibration CIRs. Such a change to the environment requires that the calibration CIRs be updated to reflect this change, which is very difficult with a person moving within the target environment. This is a primary disadvantage of this hidden Markov model for detecting changes to the CIR.

The most extreme case of choosing calibration CIRs would be to use the CIR samples that immediately precede the samples with a possible target. These calibration CIRs may include the target of interest as part of what is considered the static environment. This would minimize environmental variation that may occur over time and effectively eliminate the calibration requirement. This would also have a negative effect of biasing the target's range estimate toward the radios if the target is moving away from the radios and makes the detection of a non-moving target more difficult. However, if CIRs are sampled frequently enough relative to the person's speed, this bias toward the radios would be minimal.

In this work, we assume there are no major changes to the environment throughout each trial that would require new calibration CIRs to be captured. This allows us to use just one calibration period for estimating k_* .

TABLE II
UWB ESTIMATION PARAMETERS

Description	Parameter	Value
Voxel width [m]	p	0.15
Sampling Period [ns]	T	1
Short-term CIR variance window	N_U	5
Variance normalization parameter	β	$1/N_U$

B. Variance-based UWB Range Estimation

An alternative method is to use the short-term variance of the CIR for each r_k . We refer to this method as *VB-UWB*, or variance-based UWB. α_k is calculated as:

$$\alpha_k = \frac{\sigma_{r_k}^2}{g r_k}, \quad (17)$$

where the variance $\sigma_{r_k}^2$ is the unbiased sample variance of r_k over the N_U most recent CIRs. In this work, we let $N_U = 5$, corresponding to the number of CIRs captured in approximately 0.5 s. The normalization coefficient g is calculated as:

$$g = g(1 - \beta) + r_k \beta. \quad (18)$$

This is equivalent to applying a low-pass IIR filter to r_k . In this work, $\beta = \frac{1}{N}$. Because the variance of r_k is high when the mean of r_k is high and vice versa, we normalize the variance $\sigma_{r_k}^2$ by the mean of r_k . In this way, α_k increases only when the person moves. This method is used in conjunction with the variance-based RTI method described in Section II-A. The primary advantage of this method is that no calibration is required to solve for α_k . A disadvantage is that the target can disappear if it remains motionless over a long period of time. We alleviate this problem by applying the methods in Section V.

C. UWB Image Estimation

When estimating the UWB image, the image space is constrained to contain only the inner dimensions of the target room plus one additional voxel on each image edge. Discretizing the image space into N voxels, the image vector is:

$$\mathbf{l}^u = [l_1^u, \dots, l_N^u]^T, \quad (19)$$

where each voxel l_n^u has a bistatic range to the UWB transmitter and receiver described by its path delay k_n . The value of each voxel, l_n^u , is calculated as the non-negative difference function:

$$l_n^u = (\alpha_{k_n} - \alpha_{k_n-1})^+ \quad (20)$$

where the non-negative difference function is defined as:

$$(x)^+ = \begin{cases} x & \text{if } x \geq 0 \\ 0 & \text{if } x < 0 \end{cases}, \quad (21)$$

and assuming $\alpha_0 = 0$.

IV. COMBINING RTI AND UWB INFORMATION

In this section we introduce three methods to combine RTI and UWB and we compare the results of the different methods in Section VII.

A. Image Combination

An RTI image is formed as described in Section II-A after every RSS sensor has transmitted a packet on all channels in \mathcal{F} , i.e., after RSS measurements have been collected on all the links and channels. A UWB image is formed for every new CIR captured. The two images are combined to form the new image L^c by performing a voxel-wise product,

$$L^c = l^r \wedge l^u. \quad (22)$$

where $l^r = \hat{\mathbf{x}}$ from Equation (9) and l^u is from the UWB image \mathbf{l}^u . We define $M_{L^c} = \max L^c$. When no person is located in the monitored area, M_{L^c} has a very low value. We use a threshold T_e to avoid further processing images not showing the presence of a person in the target area: if $M_{L^c} \leq T_e$, we discard the current combined image and wait for the next one formed by the system. Otherwise, we normalize the values of the voxels of l^r and l^u such that their minimum value is zero and the sum of all voxels is one:

$$[\hat{l}^r]_n = \frac{l_n^r}{\sum_{i=1}^N l_i^r}, \quad (23)$$

and similarly for l^u :

$$[\hat{l}^u]_n = \frac{l_n^u}{\sum_{i=1}^N l_i^u}. \quad (24)$$

The normalization brings the two images in the same range of values and weights them equally. The normalized combined image \hat{L}^c is calculated again by performing a voxel-wise product of \hat{l}^r and \hat{l}^u :

$$\hat{L}^c = \hat{l}^r \wedge \hat{l}^u. \quad (25)$$

The RSS and UWB data collected by the two systems are time stamped to allow synchronizing the two images. Images are formed at the same rate as the higher of the two sampling rates. In our case, since the UWB CIRs are sampled more frequently than each RTI cycle, a combined image is formed for each new UWB sample. This image will then be the combination of the most recently formed RTI with the new UWB image. From the normalized combined image, \hat{L}^c , the position of the person is estimated as:

$$\hat{p} = \arg \max_{n \in N} \hat{L}^c, \quad (26)$$

i.e., the person's position estimate is at the voxel n having the highest value.

B. Linear Inversion with UWB Data

An alternative method to form a combined localization image is to modify the weight W matrix in (1) to include the UWB measurements in the inversion process. We define the matrix \mathbf{W}_U is an $M \times N$ matrix where M is the maximum value of k and N is the number of voxels of the image. Each column of \mathbf{W}_U represents the ideal vector of α_k if the target were located at voxel p . The vector y_U is the estimated vector

of α_k from the results of the forward-backward algorithm. Equation (1) then becomes:

$$\begin{bmatrix} \mathbf{y}_R \\ \mathbf{y}_U \end{bmatrix} = \begin{bmatrix} \mathbf{W}_R \\ \mathbf{W}_U \end{bmatrix} \mathbf{x} + \begin{bmatrix} \mathbf{n}_R \\ \mathbf{n}_U \end{bmatrix} \quad (27)$$

where the subscripts R and U correspond to the matrices derived from the RSS or UWB data, respectively. The inversion matrix is calculated as described in Section II-C using the combined \mathbf{W}^C matrix. A combined localization image \hat{L}^c is then formed by multiplying the inversion matrix in (10) to the combined RSS and UWB measurement matrix \mathbf{y}^c . The position of the person is estimated as in (26).

C. Estimating X by using Y

Another method for combining the UWB and RTI images is to derive one coordinate of the position estimate of a target from each image. First, we estimate the target location from the RTI image formed as described in Section II-A. The y -coordinate from this position estimate is used to derive an x -coordinate from the UWB image, which is calculated as described in III-C. If the target location estimate from the RTI image is at coordinates (\hat{x}^R, \hat{y}^R) , we consider the row of the UWB image corresponding to \hat{y}^R . The target position estimate \hat{p} is set at the voxel having the maximum value in that row, *i.e.*, $\hat{p} = (\hat{x}^U, \hat{y}^R)$.

V. LOCALIZATION AND TRACKING

The position estimate \hat{p} is used for updating an already existing track of a person or for initiating a new one if the target area is empty. To this purpose, we use track confirmation and deletion rules [24]. If at time k the set of *candidate tracks*, \mathcal{T}_d , and the set of *confirmed tracks* \mathcal{T}_f are both empty, *i.e.*, the position estimate $\hat{p}(k)$ is used to start a new candidate track, which is added to \mathcal{T}_d . A candidate track becomes a confirmed track only if its position has been updated at least h_{app} times in the last H formed combined images ($h_{app} \leq H$). If this condition is not fulfilled, the candidate track is deleted.

A *gating area* of radius ω is centered at the target's position estimate \hat{p} . The radius ω is defined as an integer multiple of the voxel width p . If one or both of the sets \mathcal{T}_f and \mathcal{T}_c are not empty, only the tracks located within the gating area are considered for a potential association to the current position estimate. These tracks form the set $\mathcal{T}_g \subseteq (\mathcal{T}_f \cup \mathcal{T}_c)$. The confirmed tracks in \mathcal{T}_g are given priority over the candidate tracks: the current position estimate is used to update the closest confirmed track. Otherwise, if no confirmed track exists, the current position estimate is used to update the closest candidate track. If the set \mathcal{T}_g is empty, the current position estimate is used to start a new candidate track. By using the gating area, we avoid the position estimate of the person to have large sudden changes in correspondence of noisy RSS and CIR measurements from the two systems.

VI. EXPERIMENTS

The first experiment was conducted in a study room on the second floor of the Warnock Engineering Building at the

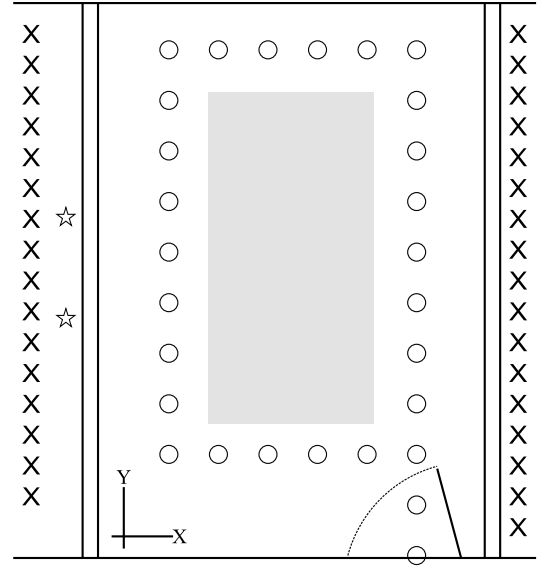


Fig. 1. Layout of the study room located in the Warnock Engineering Building at the University of Utah used for the experiments. Xs represent the 33 RSS sensors. Stars represent the 2 UWB radios. Circles represent the steps taken by the person at one second intervals. Grey rectangles represent furniture. The target room's inner dimensions are 3.82 m by 5.49 m (21 m² area).

University of Utah. A total of 33 RSS sensors were placed outside of the room along two opposite walls, 17 on one side and 16 on the other. The sensors were 30.5 cm apart. Two UWB radios were placed on one of the two sides of the room where the RSS sensors were positioned. The UWB radios were 1 m apart. A person walked along a predefined path six times, three times counter-clockwise and three times clockwise. The person entered and exited the room in each of the six trials. With the help of a metronome and markings on the floor, the person walked at a constant speed of 0.5 m/s. Figure 1 shows the setup of the tests carried out in the study room.

The second experiment was conducted in a room of a motel in Salt Lake City, Utah. The layout of this room is described in Figure 2. This time, ten RSS sensors were placed along each of the walls separating the room from the adjacent ones. Two UWB radios were placed outside one wall of the target room. The experiments were conducted with the UWB radios at two different distances, 0.9 m and 2.7 m apart. A person walked along a predefined path at a constant speed of 0.5 m/s, entering and exiting the room each trial. There were no other rooms adjacent to the target room besides the two where sensors were placed. For the second experiment, a person walked the target path 18 times. Six of the trials were done with the UWB radios in configuration A and twelve in configuration B, represented by white stars and black stars, respectively, in Figure 2. A photo of the interior of the target room can be seen in Figure 3.

VII. RESULTS

For the first experiment, 50 simulations were run using randomly selected subsets of S RSS sensors available on each

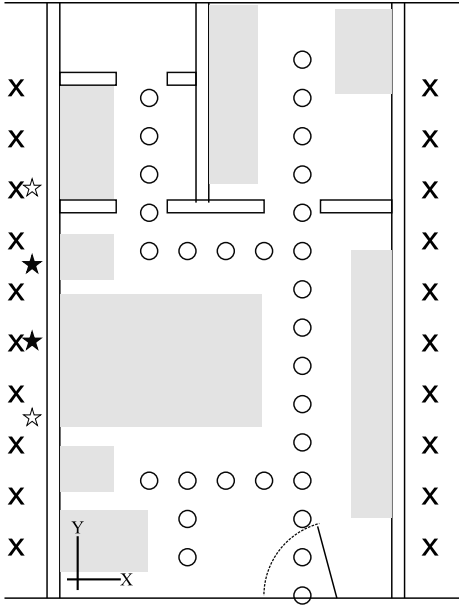


Fig. 2. Layout of the room of a motel located in Salt Lake City, Utah. Xs represent the RSS sensors. White and black stars represent the UWB radios in configurations A and B, respectively. Circles represent the steps taken by the person at one second intervals. Grey rectangles represent furniture. The target room's inner dimensions are 3.96 m by 7.11 m (28 m² area).



Fig. 3. Photo of the interior of the motel room where the second experiment was conducted.

side of the room. The density of sensors on each side of the target room is higher than what would be used in a typical deployment. Subset sizes for these simulations ranged from 3 to 10 sensors per side. The same number of sensors were used on each side of the room. The same subset of sensors was used for each of the six trials and remained the same when UWB radio data was included for a given simulation. The gating algorithm described in Section V was applied in all simulations. Simulations were performed using AB-RTI, AB-RTI with HMM-UWB, VB-RTI, and VB-RTI with VB-UWB.

Figure 4 shows the mean RMS localization error for each of the methods used measured. Each point on the figure is the error is averaged over the 50 simulations and 6 trials performed for this experiment using S sensors.

The Y-axis error improves significantly with each additional

sensor used on each side of the room. There is also little improvement in the Y-axis error as a result of including the UWB information. This is the expected behavior of the system. Variance-based methods show improvement in reducing Y error over attenuation-based methods. The X-axis error improves as a result of including more sensors on each side of the room but not as greatly as does the Y-axis error. The improvement as a result of including UWB information, however, is much more significant and is also almost constant as a function of the number of RSS sensors. The localization error improves overall, that is, as a Euclidean distance, by 51 cm and 33 cm, on average, for attenuation and variance-based methods, respectively.

As a point of comparison, if a point in the room is selected at random at each time, the RMS L2 error is 2.94 m on average over the 6 trials. Errors for the X and Y axes by selecting random locations are 1.65 m and 2.44 m, respectively. The gating algorithm is not applied when performing estimating location using random coordinates.

For the second experiment, 50 simulations were also run using randomly selected subsets of S RSS sensors on each side of the room for each simulation. When $S = 10$, however, only one simulation was performed because there was only one possible combination of $S = 10$ radios per side. For each simulation, localization is performed using AB-RTI, AB-RTI with HMM-UWB, VB-RTI, and VB-RTI with VB-UWB. The gating algorithm described in Section V is also applied to each of these methods. Figures 5 shows, from left to right, the L2, X, and Y errors when applying these four methods to the data collected over the 18 trials performed in the motel room.

One noticeable difference between the results of the two experiments is that the Y error in the second experiment degrades significantly by including VB-UWB with VB-RTI whereas for the first experiment the Y error was effectively the same. Generally, however, the same trends are visible in the results for the second experiment. The Y error improves with increasing S and including UWB data significantly improves X error.

For the second experiment, the error using 10 sensors per side is higher than the error using 7 sensors, in many cases. There were only 10 sensors on each side of the room and, therefore, only one unique simulation could be performed using 10 sensors. By performing many simulations using subsets of the available sensors, the effects due to sensor placement on localization error could be minimized. This was not possible in the case where $S = 10$ for the second experiment.

Table III shows the mean RMS error over the 18 trials performed for this experiment using all 20 RSS sensors. For comparison and as an estimate of the upper bound on error for a given environment and target path, random image coordinates are selected as the target location estimate. At each time when a combined image would be formed, X and Y coordinates and randomly selected and are used as the location estimate at that time. The gating algorithm described in Section V is not applied when randomly choosing location

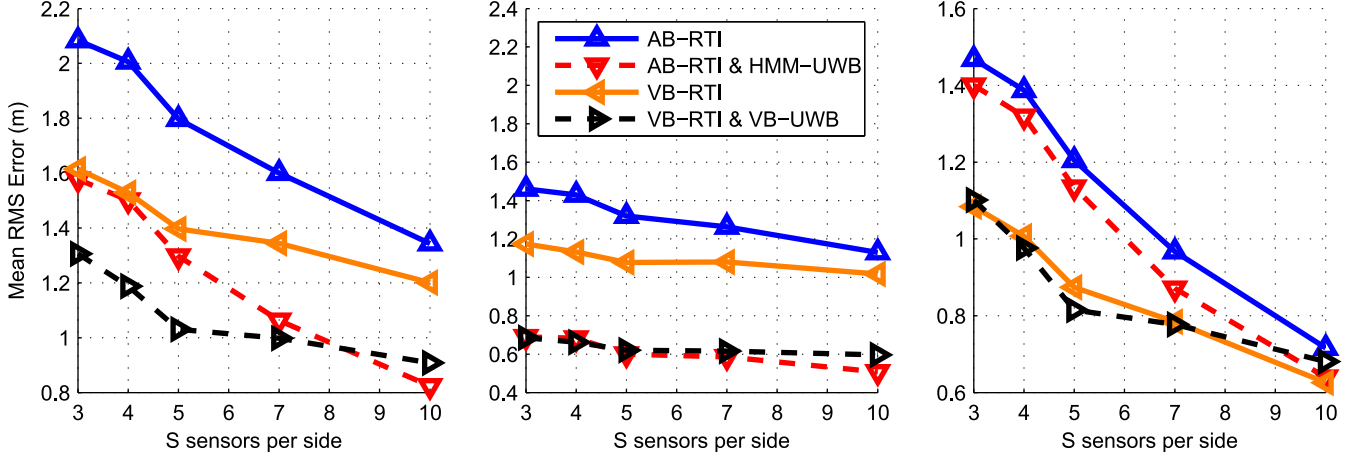


Fig. 4. From left to right, the mean RMS L2, X, and Y errors over the 6 trials and 50 simulations using random subsets of S sensors per side of the study room.

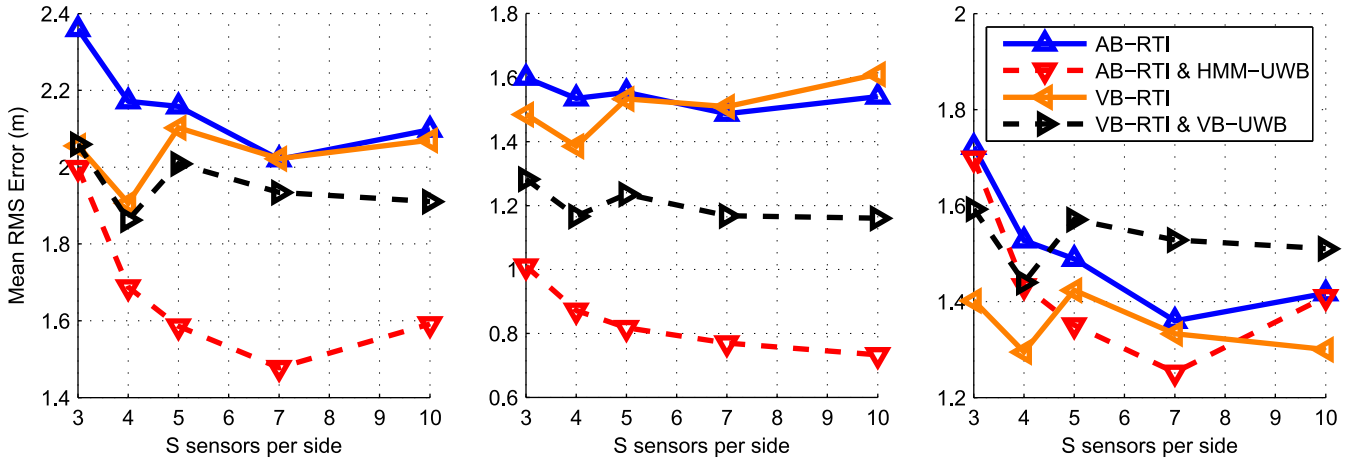


Fig. 5. From left to right, the mean RMS L2, X, and Y errors over the 18 trials and 50 simulations using random subsets of S sensors per side of the motel room. When $S = 10$, only 1 simulation was performed.

estimates. The results from applying the methods described in Sections IV-B and IV-C are also given in Table III.

Note in Table III that when performing localization using AB-RTI or VB-RTI, the X-axis error is about the same as that obtained from randomly guessing an X coordinate for each image. This is critically important for tactical operations. Having some knowledge about the person's coordinate in each axis is essential for law enforcement personnel to be able to make tactical decisions.

A. Area of Uncertainty

We define the area of uncertainty (AoU) as the ratio of the L2 mean squared error (MSE) to the total area of the monitored room:

$$AoU = \frac{L2 \text{ MSE}}{\text{Room Area}}. \quad (28)$$

Table IV shows the percent reduction in the AoU by adding UWB data to AB-RTI and VB-RTI for $S = 3$ and $S = 10$ sensors.

TABLE IV
PERCENT REDUCTION OF AoU BY INCLUDING UWB DATA.

	Study Room		Motel Room	
	AB-RTI	VB-RTI	AB-RTI	VB-RTI
$S = 3$	40.2%	32.4%	26.3%	0.2%
$S = 10$	61.8%	43.2%	41.3%	14.9%

The percent reduction in the AoU is significant except for VB-RTI in the motel room using 3 sensors. This may be due to the particular subsets of sensors used in the simulations when $S = 3$. The reduction in the AoU confirms that by adding UWB data the system can more accurately indicate to law enforcement personnel in which part of the room the person is located.

VIII. CONCLUSIONS

In this work, we present a joint DFL system that uses the changes measured in RSS and UWB CIR to localize and

TABLE III

MEAN RMS LOCALIZATION ERROR FOR THE SECOND EXPERIMENT OVER ALL 18 TRIALS FOR THE METHODS DESCRIBED. GATING WAS USED FOR ALL METHODS EXCEPT RANDOM SELECTION. UNITS GIVEN IN METERS.

	AB-RTI	AB-RTI & HMM-UWB	VB-RTI	VB-RTI & VB-UWB	Inversion with UWB	X from Y	Random
L2	2.10	1.59	2.07	1.91	1.84	1.76	3.31
X	1.54	0.73	1.61	1.16	1.31	0.98	1.53
Y	1.42	1.41	1.30	1.51	1.28	1.44	2.94

track a person through walls. We target tactical operations and crisis situations where it is not possible for the police forces to place sensors on all sides of the area to be monitored. Experimental results show that including UWB with RSS data significantly improves localization accuracy when RSS sensors are only available on two sides of the target area. Where RSS sensors have been placed along the Y axis, improvements in accuracy along the X axis by including UWB data are especially significant. Without including UWB data, the accuracy along the X axis can be as bad as randomly guessing an X coordinate.

We introduce three methods to combine the information from the UWB and RSS systems and we compare their performance. The multi-channel variance-based RTI method proposed in this work, which does not require an initial calibration in stationary conditions, is as effective or more effective than attenuation-based RTI for through-wall localization. The improvements in localization accuracy and the reduction in the AoU demonstrate that UWB data should be included in a DFL system for tactical operations where RSS sensors may only be placed on two sides of a room.

REFERENCES

- [1] J. Wilson and N. Patwari, "See-through walls: Motion tracking using variance-based radio tomography networks," *Mobile Computing, IEEE Transactions on*, vol. 10, no. 5, pp. 612–621, May 2011.
- [2] N. Bond, "Ogden Standoff ends with gun shots," <http://www.abc4.com/s/RcPlwoCoB0yBw4mhq56SiA.csp>, Jun 2011.
- [3] A. Falk, "Police arrest two after hotel standoff," <http://www.sltrib.com/sltrib/home/51277562-76/police-hotel-lake-salt.html.csp>, Feb 2011.
- [4] J. Smith, "14-hour standoff ends with arrest," <http://www.deseretnews.com/article/700052528/14-hour-standoff-ends-with-arrest.html>, Jul 2010.
- [5] M. Youssef, M. Mah, and A. Agrawala, "Challenges: device-free passive localization for wireless environments," in *MobiCom '07: ACM Int'l Conf. Mobile Computing and Networking*, 2007, pp. 222–229.
- [6] J. Wilson and N. Patwari, "Radio tomographic imaging with wireless networks," *Mobile Computing, IEEE Transactions on*, vol. 9, no. 5, pp. 621–632, May 2010.
- [7] N. Patwari and J. Wilson, "RF sensor networks for device-free localization and tracking," *Proceedings of the IEEE*, vol. 98, no. 11, pp. 1961–1973, Nov. 2010.
- [8] O. Kaltiokallio and M. Bocca, "Real-time intrusion detection and tracking in indoor environment through distributed rssi processing," in *Embedded and Real-Time Computing Systems and Applications (RTCSA), 2011 IEEE 17th International Conference on*, vol. 1, Aug. 2011, pp. 61–70.
- [9] N. Patwari and P. Agrawal, "Effects of correlated shadowing: Connectivity, localization, and RF tomography," in *IEEE/ACM Int. Conf. on Information Processing in Sensor Networks (IPSN'08)*, April 2008, pp. 82–93.
- [10] J. Wilson and N. Patwari, "A fade-level skew-laplace signal strength model for device-free localization with wireless networks," *IEEE Transactions on Mobile Computing*, vol. 11, no. 6, pp. 947–958, Jun. 2012. [Online]. Available: <http://dx.doi.org/10.1109/TMC.2011.102>
- [11] R. Thoma, O. Hirsch, J. Sachs, and R. Zetik, "Uwb sensor networks for position location and imaging of objects and environments," in *The Second European Conference on Antennas and Propagation, 2007. EuCAP 2007.*, Nov. 2007, pp. 1–9.
- [12] S. Bartoletti and A. Conti, "Passive network localization via uwb wireless sensor radars: the impact of toa estimation," in *2011 IEEE International Conference on Ultra-Wideband (ICUWB)*, Sept. 2011, pp. 258–262.
- [13] M. McCracken and N. Patwari, "Hidden Markov estimation of bistatic range from cluttered ultra-wideband impulse responses," in *2nd IEEE Topical Meeting on Wireless Sensors and Sensor Networks (WiSNet 2012)*, Jan. 2012.
- [14] <http://www.cambridgeconsultants.com/prism>.
- [15] <http://www.camero-tech.com/Index.php>.
- [16] <http://www.timedomain.com/p400-mrm.php>.
- [17] O. Kaltiokallio, M. Bocca, and N. Patwari, "Enhancing the accuracy of radio tomographic imaging using channel diversity," in *9th IEEE International Conference on Mobile Ad hoc and Sensor Systems*, Oct 2012.
- [18] O. Kaltiokallio, M. Bocca, and N. Patwari, "Follow @grandma: Long-term device-free localization for residential monitoring," in *7th IEEE International Workshop on Practical Issues in Building Sensor Network Applications*, October 2012.
- [19] Texas Instruments. A USB-enabled system-on-chip solution for 2.4 GHz IEEE 802.15.4 and ZigBee applications. [Online]. Available: <http://www.ti.com/lit/ds/symlink/cc2531.pdf>
- [20] Y. Zhao and N. Patwari, "Noise reduction for variance-based device-free localization and tracking," in *8th IEEE Conference on Sensor, Mesh and Ad Hoc Communications and Networks (SECON'11)*, June 2011.
- [21] L. Rabiner, "A Tutorial on Hidden Markov Models and Selected Applications in Speech Recognition," *Proceedings of the IEEE*, vol. 77, no. 2, pp. 257–286, Feb. 1989.
- [22] T. Cover and J. Thomas, *Elements of Information Theory*, 2nd ed., ser. Wiley Series in Telecommunications and Signal Processing. Hoboken, NJ: Wiley-Interscience, 2006.
- [23] M. McCracken and N. Patwari, "Hidden markov estimation of bistatic range from cluttered ultra-wideband impulse responses," <http://arxiv.org/abs/1212.1080>, Dec 2012.
- [24] S. Blackman and R. Popoli, *Design and Analysis of Modern Tracking Systems*. Artech House Publishers, 1999.